Modelling and numerical analysis of a parabolic system describing a binary alloy solidification process *

D. Kessler † O. Krüger † J. Rappaz † J.F. Scheid ‡

Abstract

We study a phase-field model describing the isothermal solidification process of a binary alloy. We derive a thermodynamically consistent phase-field model based on Warren and Boettinger. A formal asymptotic analysis relates this diffuse-interface model to sharp-interface Stefan-like problems. We introduce a finite-element in space, semi-implicit in time numerical scheme, and prove its convergence. Numerical tests verify the theoretical convergence results. Finally, an adaptive mesh strategy allows us to simulate dendritic growth.

Key words: phase-field model, parabolic systems.

AMS subject classifications: 82C26, 35K50, 65M12.

1 Solutal phase-field model

We are interested in the apparition of dendrites during the isothermal solidification process of a binary alloy in a domain Ω, as described by a solutal phase-field model of the Warren-Boettinger [8] type. This type of model describes the evolution of a relative concentration $c(x,t)$ and a phase-field $\phi(x,t)$ with thermodynamically consistent evolution equations. Our model [3] is inspired on, although not exactly the same as, Warren and Boettinger's [8]. The physical system considered is a binary alloy, i.e. a mixture of two elements A and B, in a space domain Ω. The relative concentration c of the alloy takes physical values between 0 (pure element A) and 1 (pure element B). The local solid-liquid state of the alloy is described by the phase-field ϕ, which also takes physical values between 0 (pure solid) and 1 (pure liquid). We consider the case of isothermal solidification, so that the temperature $T(x,t) = T(t)$ is assumed to be constant in space and externally imposed to the system, i.e. it is a given function of time t. The physical system is supposed to be closed, and no "phase exchange" is done with its exterior. Therefore we will consider Neumann boundary conditions for our problem. Given initial conditions $c_0(x)$ and $\phi_0(x)$, the evolution of the system inside the domain Ω, according to the second law of thermodynamics and conservation of matter, is given by partial differential equations of the form:

$$\left\{\begin{array}{l} \dfrac{1}{M}\dfrac{\partial \phi}{\partial t} = \operatorname{div}\left(A(\nabla\phi)\nabla\phi\right) - \dfrac{1}{\delta}\dfrac{\partial f}{\partial \phi}(c,\phi), \\ \dfrac{\partial c}{\partial t} = \operatorname{div}\left[\mu(c,\phi)\left(\dfrac{\partial^2 f}{\partial c^2}(c,\phi)\nabla c + \dfrac{\partial^2 f}{\partial c\,\partial\phi}(c,\phi)\nabla\phi\right)\right], \end{array}\right. \tag{1}$$

where f is a free energy density, μ is linked to a variable concentration diffusion coefficient

$$D_1(\phi) = \mu(c,\phi)\,\frac{\partial^2 f}{\partial c^2}(c,\phi), \tag{2}$$

*supported by the Swiss National Science Foundation

†Département de mathématiques, EPFL,1015 Lausanne, Switzerland, `http://dmawww.epfl.ch/rappaz.mosaic/index.html`

‡Institut Elie Cartan, B.P. 239, 54506 Vandoeuvre-les-Nancy Cédex, France, jean-francois.scheid@iecn.u-nancy.fr

whereas $A(\nabla\phi)$ is an anisotropy tensor, δ the interface thickness and M a model parameter. For the mathematical and numerical analysis, we will consider the isotropic model where $A(\nabla\phi) \equiv 1$. A variable anisotropy coefficient A is introduced for simulations of dendritic growth, and accounts for the existence of privileged directions for solidification due to microscopic crystal growth.

To complete the model, a free energy density f must be constructed, and other model functions and parameters must be adjusted to physical constraints. This is done in [3], where we choose

$$f(c,\phi) = \frac{\alpha(c)}{\delta} g(\phi) + \beta(c)p(\phi) + \frac{1}{\gamma}\left[(1-c)\ln(1-c) + c\ln c\right] + f_0(c), \tag{3}$$

$$\mu(c,\phi) = \gamma c(1-c)D(\phi) \tag{4}$$

and

$$D_1(\phi) = D_s + q(\phi)\left(D_l - D_s\right). \tag{5}$$

The functions g, p and q are chosen as the simplest polynomials on ϕ that follow certain constraints such that the model becomes thermodynamically consistent. We can choose $g(\phi) = \phi^2(1-\phi)^2$ and $p(\phi) = q(\phi) = \int_0^\phi g(s)\,ds / \int_0^1 g(s)\,ds$. Functions α and β are affine in c, and they are linked, as well as γ, to physical parameters such as the pure elements melting temperatures T_m^A and T_m^B, their surface tensions σ^A and σ^B, and the interface thickness δ. Parameters D_s and D_l are respectively the solid and liquid matter diffusion coefficients. Note that the phase field diffusion coefficient M is the only model parameter not to be directly linked to physical quantities.

The evolution equations are physically intuitive when written as the set of two equations (1) for the variables ϕ and c. This form of the equations is absolutely necessary for the asymptotic analysis presented on section 2. Nevertheless, we introduce now an alternate formulation in a vectorial form, better adapted for mathematical studies. This will be especially useful on section 4. For this purpose we define the vectorial variable $\vec{u} = (\phi, \alpha c)$, where α is an arbitrary positive number chosen in such a way that the vectorial problem can be written as a uniform parabolic system of the form:

$$\frac{\partial \vec{u}}{\partial t} - \operatorname{div}\left(D(\vec{u})\nabla\vec{u}\right) = \vec{F}(\vec{u}), \tag{6}$$

where

(H1) D is a 2x2 triangular matrix and $\vec{F}$ a 2-vector of Lipschitz bounded components.

(H2) The coefficients of D are given by $d_{11} = M$, $d_{12} = 0$, $d_{21} = \alpha D_2(\vec{u})$ and $d_{22} = D_1(\vec{u})$, where M is a positive constant, $D_1(\vec{u})$, $D_2(\vec{u})$ are Lipschitz bounded functions and $D_1(\vec{u})$ is lower bounded by a positive constant.

When α is chosen small enough, then D satisfies the following uniform positive definiteness condition :

$$\exists \nu > 0 \quad \text{s.t.} \quad D(\vec{\xi})\,\vec{\zeta}\,.\,\vec{\zeta} \geqslant \nu\,\vec{\zeta}\,.\,\vec{\zeta}, \quad \forall \vec{\xi}, \vec{\zeta} \in \mathbb{R}^2. \tag{7}$$

This parabolic equation is coupled with Neumann homogeneous boundary conditions and appropriate initial conditions on $\vec{u}$.

2 Sharp-interface limits

We have formally shown in [2] that on the asymptotic limit where the interface-width δ becomes small, our model (1) behaves as a Stefan-like model with diffusion equations for c on pure solid and pure liquid regions, coupled to the motion of a sharp interface between these regions. We have derived four limit models, for different behaviours of other model parameters when δ tends to 0. We have used techniques similar to those formerly used by Caginalp [1] for thermal phase-field models, and later by Wheeler, Boettinger and McFadden [9] for a simpler solutal phase-field model.

The limit problems for the evolution equations (1) when the interface thickness δ vanishes, are all of the generic form

$$
(8)\qquad \begin{cases}
\dfrac{\partial c}{\partial t} = D_l \triangle c, & \text{in } \Omega_l, \qquad (a)\\[2mm]
\dfrac{\partial c}{\partial t} = D_s \triangle c, & \text{in } \Omega_s, \qquad (b)\\[2mm]
-v_n\, [c]_l^s = \left[D\, \dfrac{\partial c}{\partial n} \right]_l^s, & \text{on } \Gamma, \qquad (c)\\[2mm]
[f_c]_l^s = 0, & \text{on } \Gamma, \qquad (d)\\[2mm]
[f - f_c c]_l^s = \mathcal{F}(v_n, \kappa), & \text{on } \Gamma, \qquad (e)
\end{cases}
$$

where Ω_l and Ω_s are respectively pure liquid and pure solid regions, separed by an interface Γ.

In all of these limits, pure liquid $(8.a)$ and pure solid $(8.b)$ regions with classical diffusion coexist, separed by sharp interfaces that evolve ensuring the conservation of matter $(8.c)$. Besides, the values of concentration at the interface can be obtained through a "parallel tangent construction" $(8.d\text{-}e)$, using solid and liquid free energy densities, and dependent either on the local interface velocity v_n, the local interface curvature κ, both or none, through the generic linear function $\mathcal{F}(v_n, \kappa)$. This function is dependent on the type of limit :

(9)

limit	σ_A, σ_B	$\dfrac{\sigma_A}{T_m^A} - \dfrac{\sigma_B}{T_m^B}$	M	$\mathcal{F}$
1	$\sim \delta$	$\sim \delta$	~ 1	0
2	$\sim \delta$	$\sim \delta$	$\sim \delta$	$\sim\ v_n$
3	~ 1	$\sim \delta$	~ 1	$\sim\ \kappa + v_n/M$
4	~ 1	$\sim \delta$	$\sim 1/\delta$	$\sim\ \kappa$

3 Mathematical analysis

We have established the following results in [6]:

- *Existence Result*:

  Under assumptions (H1)-(H2), when $\Omega \subset \mathbb{R}^d$, $d = 2, 3$, is a regular domain and for any $\vec{u}_0 \in L^2(\Omega)$ and $T > 0$, problem (1) with $A(\nabla\phi) \equiv 1$ admits a (weak) solution $\vec{u} \in L^2(0, T; H^1(\Omega)) \cap L^\infty(0, T; L^2(\Omega)) \cap H^1(0, T; (H^1(\Omega))')$.

- *Maximum principle* (for the underlying physical variables): Under the assumptions required for the existence result, if furthermore $\vec{F}(\vec{u})$ and the $D_2(\vec{u})$ are equal to zero when $u_1 = \phi$ is outside the interval $[0, 1]$, we have the following result: Let $\phi_0, c_0 \in L^2(\Omega)$ with $0 \leqslant \phi_0, c_0 \leqslant 1$ a.e. in Ω.

  Then every (weak) solution of problem (1) satisfies $0 \leqslant \phi, c \leqslant 1$ a.e. in $\Omega \times (0, T)$.

  Note that the assumed truncation of functions $\vec{F}(\vec{u})$ and $D_2(\vec{u})$ does not contradict the physical model, in which all quantities are only defined for $\phi \in [0, 1]$, and can be given any arbitrary shape outside of this physical interval.

The existence result has been established using a Faedo-Galerkin method. Note that the maximum principle ensures that c and ϕ will always take physical values in all the domain, as long as the initial conditions do.

4 Numerical scheme, analysis and simulations

Assuming that Ω is a polygonal domain, we approximate the problem (6) by a $\mathbb{P}_1$ finite element in space, semi-implicit in time, discretization of the form:

$$
(10)\qquad \int_\Omega \frac{\vec{u}_h^n - \vec{u}_h^{n-1}}{\tau} . \vec{v}_h + \int_\Omega D(\vec{w}_h^n) \nabla \vec{u}_h^n : \nabla \vec{v}_h = \int_\Omega \vec{F}(\vec{u}_h^{n-1}) . \vec{v}_h, \qquad \forall \vec{v}_h \in V_h^2, \quad n = 1, \ldots, N,
$$

where $\vec{w}_h^n = (u_{1h}^n, u_{2h}^{n-1})$, h is the mesh size of a triangulation defining the $\mathbb{P}_1$ finite element space V_h, and τ the time step of the discretization.

Since D is lower triangular, and d_{11} is independent of $\vec{u}$, it is at each time step possible to first solve the first equation, given by (10) by chosing $\vec{v}_h = (v_{1h}, 0)$, which will therefore be linear in u^n_{1h}, and then use this value in the second equation, given by (10) by chosing $\vec{v}_h = (0, v_{2h})$, which will also be linear in u^n_{2h}. Thus, the semi-implicity of the scheme avoids having to solve non-linear algebraic equations at each time step. We have shown in [4] that:

- *A priori error estimate*: Under assumptions `(H1)-(H2)`, if $\Omega \subset \mathbb{R}^2$ is a convex polygonal domain, if the mesh is regular and satisfies an inverse assumption and if $\vec{u} \in H^1(0, T, W^{1,\infty}(\Omega) \cap H^2(\Omega))$ then

  (11) $$||\vec{u}(t_n) - \vec{u}^n_h||_0 \leqslant C(h^2 + \tau), \quad n = 0, \dots, N,$$

  where $||.||_0$ stands for the L^2 norm.

The proof relies on the introduction of a generalized vectorial elliptic projector, using techniques based on those of V. Thomée [7], using a generalized vectorial elliptic projector $\pi_h : H^1(\Omega, \mathbb{R}^2) \to V_h^2$ defined by the following property :

(12) $$\int_\Omega D(\vec{u})\nabla(\vec{u} - \pi_h \vec{u}) : \nabla \vec{v}_h + \int_\Omega (\vec{u} - \pi_h \vec{u}).\vec{v}_h = 0, \quad \forall \vec{v}_h \in V_h.$$

The Lax-Milgram lemma ensures that $\pi_h \vec{u}$ is well-defined. Note that the second term in the left-hand side of equation (12) is necessary to account for Neumann (instead of Dirichlet) boundary conditions for $\vec{u}$ in our problem.

We have derived several useful properties of the generalized vectorial elliptic projector, estimating several norms of $\pi_h \vec{u}$ and of $\vec{u} - \pi_h \vec{u}$. The convergence result (11) is then established by estimating

(13) $$||\vec{u}(t_n) - \vec{u}^n_h||_0 \leqslant ||\vec{u}(t_n) - \pi_h \vec{u}(t_n)||_0 + ||\pi_h \vec{u}(t_n) - \vec{u}^n_h||_0.$$

The first term of the right-hand side is immediatly estimated as being of order h^2 using the projector's properties, while the last term requires some extra work, and the use of the discrete Gronwall's lemma. Details of the proof of (11) can be found on [4].

Numerical simulations have been undertaken using the numerical scheme (10). Experimental convergence order on numerical test cases coincides well with the aforementioned theoretical results, as can be seen on 1 and 2. These figures represent the logarithm of the L^2 error as a function of the logarithm of the mesh size h (resp. of the time step τ), as well as reference straight lines with slopes 1 and 2 (resp. 0.5 and 1). A least-square approximation on the three best-aligned dots of these figures gives a slope of 1.838 for figure 1, and a slope of 0.999 for figure 2, which fit well to the predicted order of convergence $h^2 + \tau$. Details of the implementation of these numerical tests can be found in [5].

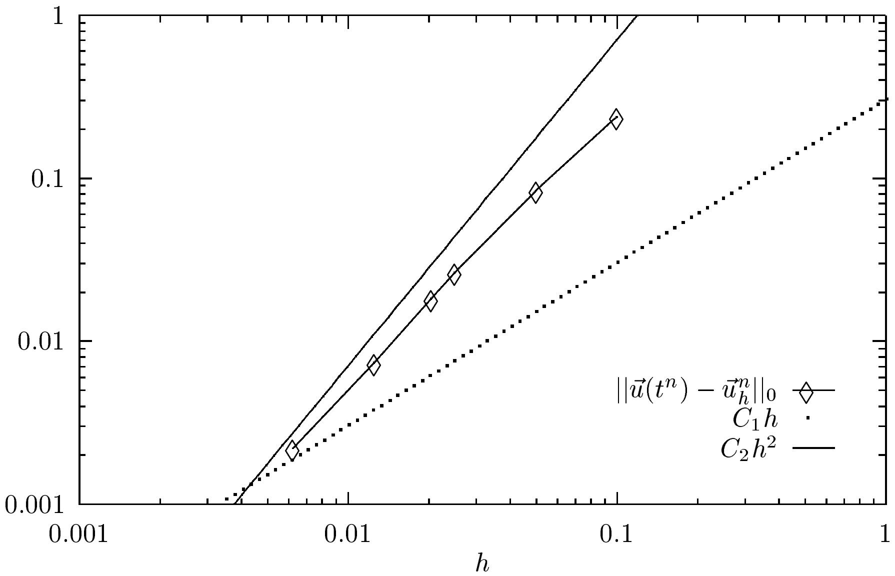

Figure 1: Numerical scheme convergence as the mesh size becomes small (with a fixed small time step)

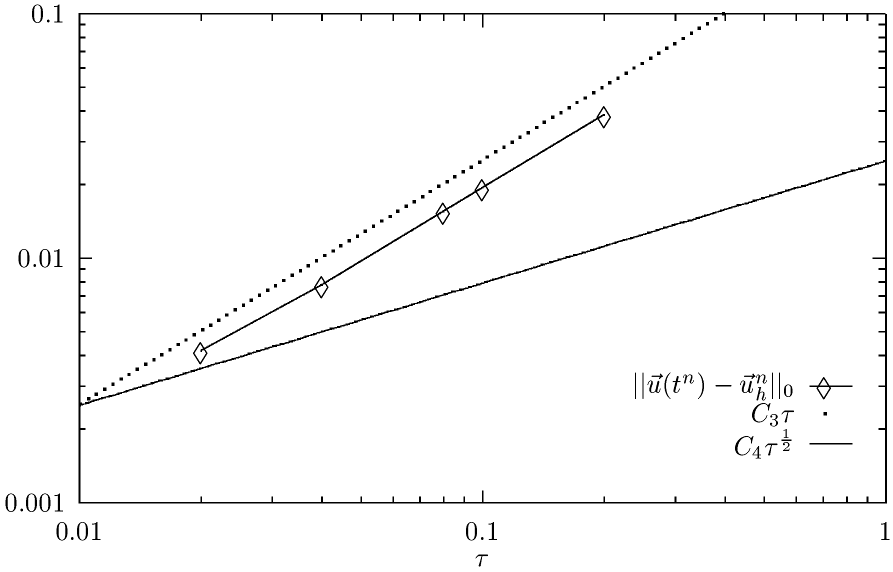

Figure 2: Numerical scheme convergence as the time step becomes small (with a fixed small mesh size)

We have also undertaken numerical simulations using an adaptive mesh strategy based on an *ad hoc* error estimator (see [5]) for the anisotropic problem. The anisotropy tensor A, accounting for privileged directions of solidification due to microscopic properties of crystal growth, is then defined as

$$A(\nabla\phi) = a^2(\theta(\nabla\phi)) \begin{pmatrix} 1 & 0 \\ 0 & 1 \end{pmatrix} - a'(\theta(\nabla\phi))a(\theta(\nabla\phi)) \begin{pmatrix} 0 & 1 \\ -1 & 0 \end{pmatrix}, \tag{14}$$

where $\theta(\nabla\phi)$ is the angle between $\nabla\phi$ and the horizontal axis, i.e. $\nabla\phi \equiv |\nabla\phi|(\cos\theta, \sin\theta)^T$. We use the phenomenological anisotropy function $a(\theta) = 1 + \bar{a}\cos(k\theta)$, where k is the order of anisotropy and $\bar{a} \in [0,1]$ determines the anisotropy amplitude.

A simulation of dendritic growth, which happens when the solidification of an alloy is anisotropic, is shown on figure 3. For this computation, model paremeters where fitted to physical values for a Ni-Cu alloy with a 4th-order anisotropy. It took about 24 hours to compute in 2000 time steps the solution represented on figure 3, using a SGI MIPS R10000 with 8 250 MHZ IP27 Processors. The numerical implementation is not yet optimal, since we used direct methods for solving linear systems. The initial condition used for this computation corresponds to a small solid disc in the middle of a homogenous liquid. The adaptive-mesh strategy used to compute this simulation allows for better precision near the solid-liquid interface, where most of the physics happen. We look forward on establishing *a posteriori* error estimates to build an estimator properly adapted to our problem, which would allow for more precise and better justified simulations of physical situations. We also want to modify the numerical implementation in order to shorten computation times.

Acknowledgements

We wish to thank Prof. M. Rappaz and the Physical Metallurgy Lab from the Materials Science Department of the Swiss Federal Institute of Technology, Lausanne, for a continuing collaborationship on the phase-field and other projects. We are also grateful to the Swiss National Science Foundation for financially supporting this project.

References

[1] G. Caginalp. Stefan and Hele-Shaw type models as asymptotic limits of the phase-field equations. *Phys. Rev. A*, 39(11):5887, 1989.

[2] D. Kessler. Sharp interface limits of a thermodynamically consistent solutal phase-field model. in preparation.

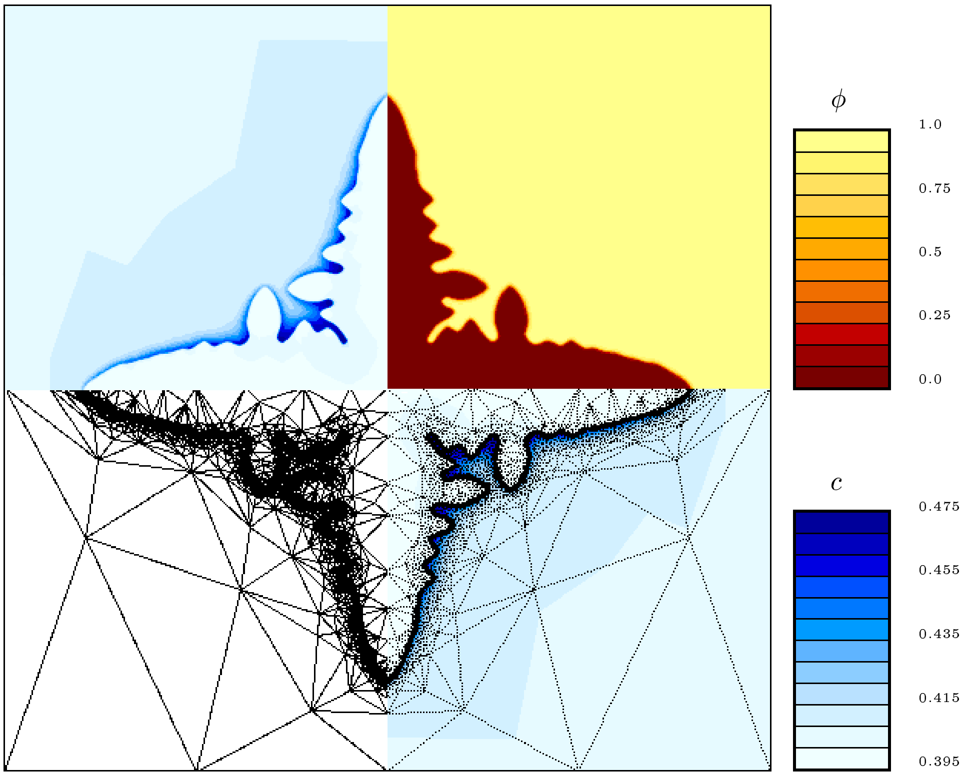

Figure 3: Simulation of dendritic growth using an adaptive mesh strategy

[3] D. Kessler, O. Krüger, and J.-F. Scheid. Construction d'un modèle de champ de phase à température homogène pour la solidification d'un alliage binaire. *DMA-EPFL internal report*, 1998.

[4] D. Kessler and J.-F. Scheid. A priori estimates for a parabolic system describing a binary alloy solidification process. in preparation.

[5] O. Krüger. *Modélisation et analyse numérique de problèmes de réaction-diffusion provenant de la solidification d'alliages binaires.* PhD thesis, EPFL, 1999.

[6] J. Rappaz and J.-F. Scheid. Existence of solutions to a phase-field model for the solidification process of a binary alloy. to appear in *Math. Methods Appl. Sci.*, 1999.

[7] V. Thomée. *Galerkin Finite Element Methods for Parabolic Problems.* Springer, 2^{nd} edition, 1991.

[8] J. A. Warren and W. J. Boettinger. Prediction of dendritic growth and microsegregation patterns in a binary alloy using the phase-field model. *Acta metall. mater.*, 43(2):689–703, 1995.

[9] A. A. Wheeler, W. J. Boettinger, and G. B. McFadden. Phase-field model for isothermal phase transitions in binary alloys. *Phys. Rev. A*, 45(10):7424–7439, 1992.